Boric Acid Removal with Polyol-Functionalized Polyether Membranes

Matthew R. Landsman[1#], Frederick Rivers[2#], Benjamin J. Pedretti[2], Benny D. Freeman[2], Desmond F. Lawler[1], Nathaniel A. Lynd[2], and Lynn E. Katz[1*]

[#]These authors contributed equally to this work (joint first authorship).

*corresponding author, lynnkatz@mail.utexas.edu, 301 E Dean Keeton Street, ECJ 9.102H, University of Texas at Austin, Austin, TX 78712 United States

[1]Department of Civil, Architectural, and Environmental Engineering, The Center for Materials for Water and Energy Systems (M-WET), University of Texas at Austin, Austin, TX 78712 United States

[2]McKetta Department of Chemical Engineering, The Center for Materials for Water and Energy Systems (M-WET), University of Texas at Austin, Austin, TX 78712 United States

Resubmitted to *Journal of Membrane Science*

August 1, 2021

Abstract

Poor selectivity of conventional desalination membranes for boron often necessitates multi-stage treatment trains to achieve desired boron removal for end uses such as irrigation. One approach to membrane design for improved single-pass boric acid removal is via incorporation of chelating ligands that selectively sorb boron. In this study, membranes based on epoxy-amine crosslinked poly(glycidyl glycidyl ether) (PGGE) were synthesized and functionalized with *N*-methyl-D-glucamine (NMDG), a polyol known to interact selectively with boron. PGGE and PGGE-NMDG membranes exhibited boron sorption isotherms that were well-described by dual mode isotherms. PGGE-NMDG sorbed 2.5 mmol B/g dry polymer from a neutral aqueous solution containing 100 mmol B/L, which was almost three times the adsorption density of a commercial boron selective resin, Amberlite IRA743. The membranes were regenerated in acid without a significant loss of boron sorption capacity over four cycles. Interactions between boron and NMDG and PGGE sites (*e.g.*, epoxides) impacted boron diffusion in both membranes. The use of ligand functionalized membranes to capture target solutes such as boron requires high loading of interacting sites to maximize uptake capacity. Establishing fundamental structure/property rules for boron selectivity could lead to new material designs with improved boron separation properties for water purification.

Keywords: poly(allyl glycidyl ether), *N*-methyl-D-glucamine, boron, water reuse, selective capture

Highlights

- PGGE membranes were synthesized and functionalized with NMDG for boron removal
- Boron sorption in the membranes was reversible and exhibited dual mode behavior
- Boron diffusion was influenced by specific interactions with PGGE and NMDG sites
- Boron capture by polyol membranes requires high capacities or frequent regeneration

Graphical Abstract

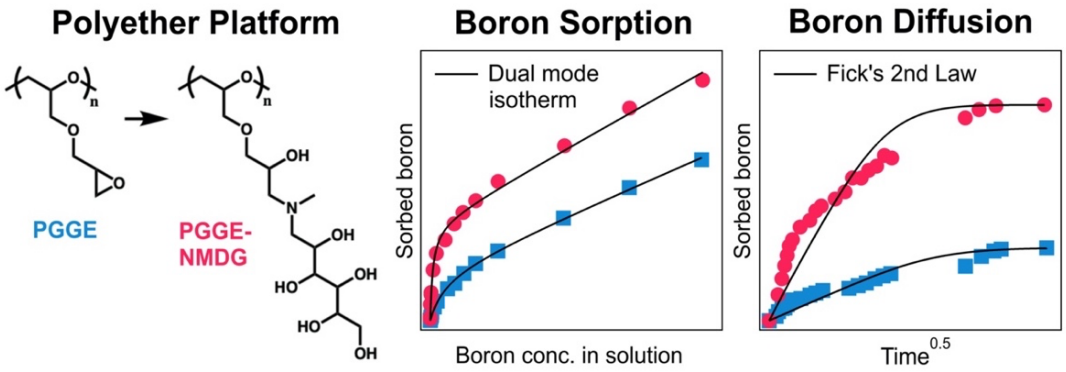

1. Introduction

Expanding current water resources to nontraditional sources of water such as seawater, brackish water, municipal/industrial wastewater, and produced water from oil/gas industries would help disrupt linkages between food, water, and energy known as the food-water-energy nexus. Membrane separation processes provide a promising option to achieve water security because they can remove a wide variety of solutes with greater energy-efficiency and smaller footprints than many traditional techniques [1]. In particular, reverse osmosis (RO) has served as a prominent technology for brackish water and seawater desalination for several decades [2,3] and it plays a key role in potable reuse of municipal wastewater [4,5]. However, a challenge limiting the potential for RO to treat unconventional waters is the removal of small, neutral solutes from such water (*e.g.*, boric acid, N-nitrosodimethylamine, 1,4-dioxane, urea). The electrostatic- and size-based interactions governing rejection of such solutes in RO membranes are weaker than those of charged and larger solutes. In particular, poor rejection of boric acid, $B(OH)_3$ – the dominant form of boron at circumneutral pH – is of great interest because boron's toxicity to some plants limits the reusability of many waters for crop irrigation [6–8]. Maximum boron concentrations in the range of 0.5–1.0 mg/L are common for irrigation of several sensitive crops (*e.g.*, wheat, beans), so boron removal during seawater desalination often requires at least 90% rejection of an influent containing 5 mg B/L [9,10]. For comparison, boron concentrations in nontraditional waters relevant to water reuse can significantly exceed maximum allowable concentrations (*e.g.*, 120 mg B/L in a produced water sample from the Eagle Ford shale play [11]; 2,000 mg B/L in an industrial wastewater from a boric acid production plant in Turkey [12]), thus favoring the development of treatment trains with superior boron removal properties.

Currently, desalination plants often employ multi-stage RO and/or post-treatment using boron-selective resins (BSRs) to meet boron removal goals. Multi-stage RO incorporates intermediate pH adjustments to convert boric acid to borate anion, $B(OH)_4^-$, because borate is more easily removed than boric acid via charge repulsion and size exclusion mechanisms (*i.e.*, the membrane rejection of borate is substantially higher than that of boric acid) [13,14]. The Ashkelon desalination plant in Israel uses a four-stage RO process with intermediate pH adjustments to achieve product water boron concentrations of <0.4 mg/L while controlling mineral scaling [15,16].

BSRs containing polyols such as *N*-methyl-D-glucamine (NMDG) remove boron via chelation due to the high affinity of vicinal hydroxyl groups for boron [17,18]. Novel BSRs have been developed that outperform commercial products in terms of boron uptake capacity and sorption rate in complex water streams [19–21], representing one approach to improving boron removal capabilities for water reuse. Moreover, process designs for membrane systems that employ BSRs in the feed water have been proposed, but industrial scale-up has been limited by operational challenges (*e.g.*, regeneration, membrane fouling) [13]. Other integrated membrane processes have also shown potential for increasing boron removal with reduced energy consumption [22] and reduced fouling [23], yet these approaches often involve increased complexity and cost. Therefore, the development of novel membranes that effectively remove boron during single-pass permeation could expand our portfolio of energy-efficient water reuse technologies.

Some membrane researchers have incorporated surface grafts on RO membranes to seal defects and improve boron rejection based on steric, electrostatic, and hydrophobic interactions at the membrane surface [24–28]. Other approaches, such as electrically conducting RO

membranes that modify pH at the interface to convert boric acid to borate, have also been proposed [29]. However, these materials are often limited by the effects of such modifications on other interfacial interactions including water flux and fouling.

Another potential approach to achieve high solute selectivity is via incorporation of chelating ligands into polymer membranes because this method leverages the selectivity of specific functional groups to modulate the transport of target solutes. This class of materials has seen extensive use in heavy metal separations [30,31], and more recently it has been proposed for several solute-specific separations in water reuse and resource recovery [32,33]. In particular, supported liquid membranes containing 1,3-diols have been used to facilitate boric acid transport during boron extraction from industrial brines [34], and porous membranes functionalized with polyols have been developed to remove boron during water purification through a capture-and-release mechanism [35–37]. Meanwhile, the incorporation of polyols in nonporous water purification membranes, where high boron rejection is imperative in applications such as seawater desalination by RO, has not been thoroughly investigated. Di Vincenzo *et al.* [38] showed NMDG-functionalized membranes to have higher boric acid rejection than a standard thin film composite membrane during dead-end filtration, and recent work by Uliana *et al.* [39] used NMDG-functionalized nonporous membranes to capture boric acid during diffusion dialysis experiments. To this end, these studies did not investigate the specific interactions between boron and the NMDG groups that influence transport. Permeation of solutes through nonporous membranes depends on sorption of the solute from the water to the membrane phase as well as diffusion of the solute through the membrane matrix [40]. The incorporation of chelating ligands in polymer membranes can influence both sorption and diffusion of solutes [33], so fundamental

investigation of the interactions between boron and NMDG as they relate to transport and selectivity is essential to designing materials in this space.

The objectives of this research were to develop a membrane platform that could be functionalized with a boron selective ligand and to evaluate the performance of such ligand-functionalized membranes relative to current boron removal sorbents. Poly(allyl glycidyl ether) (PAGE) was chosen as the membrane platform due to the functionalizable pendant allyl groups providing broad compositional versatility [41]. NMDG was chosen as the boron selective ligand due to its widespread use in BSRs and the ability to functionalize an epoxidized PAGE network with NMDG via its amine functionality. This study also investigated the boron transport mechanism within the membranes (*i.e.*, sorption and diffusion) to determine the influence of specific ligands in nonporous polymer membranes for targeted solute separations during water treatment.

2. Materials and Methods

2.1. Materials

Allyl glycidyl ether (AGE) (>99%) was purchased from TCI America (Portland, OR), dried over calcium hydride overnight, degassed, and distilled under reduced pressure. Potassium (>99%, Millipore Sigma, Burlington, MA) in mineral oil, naphthalene (98%, Millipore Sigma), benzyl alcohol (anhydrous, 99.8%, Sigma Aldrich, St. Louis, MO), methanol (certified ACS, Fisher, Waltham, MA), hydrochloric acid (37%, Millipore Sigma), dichloromethane (DCM) (certified ACS, 99.5%, Fisher), 3-chloroperoxybenzoic acid (mCPBA) (70-75% balance 3-chlorobenzoic acid and water, Fisher), 1,4-diaminobutane (Acros Organics, Fair Lawn, NJ), sodium bicarbonate ($NaHCO_3$) (Fisher), sodium sulfate (Na_2SO_4) (Fisher), and NMDG (Sigma

119 Aldrich) were all used as received. Tetrahydrofuran (THF) was collected from a J. C. Meyer dry
120 solvent system and immediately used thereafter. Deuterated chloroform ($CDCl_3$) was purchased
121 from Cambridge Isotope Laboratories, Inc (Tewksbury, MA).
122 Boric acid solutions were prepared using Milli-Q deionized (DI) water (Millipore Sigma)
123 and ACS grade $B(OH)_3$ (Sigma Aldrich). Boric acid sorption/diffusion experiments were
124 performed in 10 mM HEPES (Fisher) buffer at pH 7.0 such that boric acid was the primary
125 boron species; HEPES is a zwitterionic sulfonic acid buffering agent and is one of Good's
126 buffers [42]. A control sorption experiment used poly(ethylene glycol) diacrylate (PEGDA,
127 average M_n = 700 g/mol) (Sigma Aldrich) and phenylboronic acid (Sigma Aldrich). The nitric
128 and hydrochloric acids used in all experiments and analyses were of trace metal grade (Fisher).
129 The commercial BSR, DuPont Amberlite IRA743, was purchased from Sigma Aldrich and used
130 as received in the free base form. The Amberlite IRA743 resin is a copolymer of
131 styrene/divinylbenzene functionalized with NMDG and the average particle diameter of the resin
132 is between 500–700 μm [43–45].
133
134 *2.2. Analytical Equipment*
135 Polymers were characterized by ^1H nuclear magnetic resonance (NMR) spectroscopy and
136 gel permeation chromatography (GPC) to determine the composition, degree of
137 functionalization, and molecular weight. ^1H NMR spectroscopy was performed on a 400 MHz
138 Agilent MR spectrometer at room temperature and referenced to the residual solvent signal of
139 $CDCl_3$ (7.26 ppm). GPC was carried out on an Agilent system with a 1260 Infinity isocratic
140 pump, degasser, and thermostatted column chamber held at 30 °C containing an Agilent PLgel
141 10 μm MIXED-D column with an operating range of 200–400,000 g/mol relative to polystyrene

standards. Chloroform was used as the mobile phase. This system was equipped with an Agilent 1260 Infinity refractometer and Bio-SEC Multi-Detector suite featuring dual-angle static and dynamic light scattering detection. The kinetics of epoxy-amine polymerizations were studied by time-resolved, *in situ* Fourier transform infrared (FTIR) spectroscopy on a Mettler Toledo ReactIR 15 using a DiComp diamond probe connected via silver halide fiber optic cable with an optical range of 3000–650 cm^{-1}. Spectra were collected at room temperature and the probe was calibrated with a one-point temperature calibration. The sampling rate for spectra was one scan per minute for the first two hours and then one scan per five minutes for 18 hours. All ^{1}H NMR spectroscopy, GPC, and *in situ* FTIR data are provided in Section S1 of the Supplementary Materials.

Boron solution concentrations were determined using Inductively Coupled Plasma Optical Emission Spectrometry (ICP-OES) (Varian 710-ES, Agilent Technologies, Santa Clara, CA) in accordance with Standard Method 3120 [46]. Due to long washout times of boron in ICP, blanks were run between every sample, and standard checks and matrix spikes were used to ensure analytical accuracy. Standards were prepared in background matrices to account for potential interferences, and all regression coefficients for calibration curves and standard additions had $R^2>0.999$. To quantify the concentrations of boron in the membranes, dried membrane samples were digested in 10 M nitric acid on a Milestone ETHOS™ UP high performance microwave digestion system (Milestone, Shelton, CT). Boron concentrations in the final digestion solution were determined using ICP-OES via standard addition and converted to the boron concentration in the membrane via mass balance. Solution pH was measured using a Thermo Orion glass pH electrode (Fisher). Attenuated total reflectance-FTIR (ATR-FTIR) was employed to collect absorbance spectra of the membranes on a Thermo Scientific Nicolet 6700 with the Smart IRT™

ATR accessory (Thermo Mattson, Waltham, MA) containing a diamond crystal (penetration depth of 2.0 μm at 1000 cm^{-1}). One hundred and twenty-eight scans were collected for each spectrum and the spectra were normalized to the maximum absorbance for ease of comparison. Peak fitting of ATR-FTIR data was completed using the multi-peak fitting tool in Igor Pro (WaveMetrics, Portland, OR).

2.3. Synthesis of poly(glycidyl glycidyl ether)

Polymerization of AGE was conducted via anionic ring opening polymerization based on previously reported methods [41]. The polymerization was performed in custom, thick-walled glass reactors fitted with threaded adapters and charged with glass-coated stir bars. The reactors were first flame dried under vacuum, followed by cycling nitrogen and vacuum three times. The reactor was charged with a positive pressure (5 psig) nitrogen atmosphere and sealed from the Schlenk line. 104 μL of benzyl alcohol (0.925 mmol, 1.0 eq) was then added via a gas-tight syringe to the bottom of the reactor and deprotonated by titration with a solution of potassium naphthalenide (*ca.* 0.3 M in THF) until a light green coloration persisted, indicating complete deprotonation of the alcohol. 20.8 mL of AGE (177 mmol, 191 eq relative to benzyl alcohol) were then added via a gas-tight syringe. The reaction was allowed to proceed for 48 hours at room temperature, at which point degassed, acidified methanol (0.1 M) was added to the reaction vessel to terminate the reaction. The polymer was precipitated from excess hexanes. The supernatant was decanted and the resultant PAGE was dried overnight *in vacuo*. Number average molecular weight, M_n, determined by end group analysis by ^{1}H NMR spectroscopy was 17.0 kDa (Figure S1), while GPC results yielded M_n of 18.7 kDa and a dispersity of 1.5 relative to polystyrene standards (Figure S3).

PAGE was oxidized to poly(glycidyl glycidyl ether) (PGGE) using mCPBA. 28.1 grams of 75% mCPBA stabilized with water (131 mol, 1.3 eq) were added to a stirred solution of PAGE (10 g, 0.67 mmol, 1 eq) in DCM (100 mL) over the course of ten minutes. The reaction was allowed to stir for 24–48 hours. Once all the starting allyl groups had been converted to epoxides, as confirmed by ^{1}H NMR spectroscopy (Figure S2), the reaction mixture was filtered and washed with a saturated solution of $NaHCO_3$ (4 × 100 mL). The organic phase was then dried over Na_2SO_4, filtered, rotary evaporated, and dried *in vacuo* overnight.

2.4. Preparation of crosslinked polyether membranes

PGGE was cast with 1,4-diaminobutane and NMDG into porous polypropylene mesh that acted as mechanical support to create NMDG-functionalized polyether membranes (PGGE-NMDG). A representative sample preparation protocol proceeded as follows: First, 88.1 µL (0.88 mmol, 0.2 eq) of 1,4-diaminobutane was added to a solution of PGGE (1.0 g, 0.07 mmol, 1.0 eq) in THF (1.12 mL). For the NMDG-functionalized membranes, 0.19 g of NMDG (0.97 mmol) dissolved in 1.0 mL DI water was also added to the reaction mixture. This amount was chosen to match the boron uptake capacity of the commercial Amberlite IRA743 assuming 1:1 boron-NMDG binding stoichiometry based on a previously-reported capacity (0.99 mmol B/g dry polymer) [21]. After briefly stirring, the solution was poured onto the polypropylene mesh support placed on a quartz plate. Aluminum spacers (0.45 mm thick) were placed underneath the support to maintain uniform casting thickness. The solution was dispersed evenly on the mesh via a Teflon roller to assure solution uniformity in the mesh. The casting solution was then left to react while evaporating overnight. Water and boron sorption and diffusion data were normalized based on the polymer phase alone according to a previously reported method [47], and the

polypropylene support exhibited no water or boron uptake. See Section S2 of the Supplementary Materials for more information on the porous polypropylene support membranes.

2.5. Water uptake measurements

Water uptake of the membrane samples was measured based on a general liquid sorption measurement technique in which the mass of a circular membrane sample was determined after soaking the sample in DI water for at least 24 h and after drying the sample under vacuum at ambient temperature for at least 24 h [48]. Water uptake in the membranes was the same for measurements in DI water and 10 mM HEPES. Water volume fraction in the hydrated polymer was determined based on volume additivity using a density determination kit (Part 238490, Mettler Toledo, Columbus, OH) at ambient conditions with heptane as the auxiliary solvent, per a previously-reported method [49].

2.6. Equilibrium boron sorption experiments

Dried samples of PGGE and PGGE-NMDG membranes and Amberlite IRA743 were weighed in polypropylene vials and hydrated for 24 h in a background matrix of 10 mM HEPES (pH 7.0). Then, the batch reactors were spiked with a boric acid stock solution (500 mM, pH 7.0) to obtain desired initial concentrations (0.01–100 mM) and shaken for 48 h at room temperature. Solutions were then filtered through 0.22 μm polyethersulfone filters (Foxx Life Sciences, Salem, NH) and concentrations of boron in the initial and equilibrium solutions were determined via ICP-OES. Boron uptake, q_e (mmol B/g dry polymer), of the materials was calculated by:

$$q_e = \left(C_0 - C_{eq}\right)\frac{V}{M} \quad (1)$$

where C_0 and C_{eq} are the concentrations of boron in the initial and equilibrium solutions (mmol/L), respectively, V is the solution volume (L), and M is the dry mass of the polymer (g). Equilibrium boron sorption data for PGGE and PGGE-NMDG membranes were fit to the dual mode sorption isotherm [50]:

$$q_e = q_{Diss} + \sum_{i=1}^{n} q_{i,Lang} = K_{Diss} C_{eq} + \sum_{i=1}^{n} \frac{q_{i,max} K_{i,Lang} C_{eq}}{1 + K_{i,Lang} C_{eq}} \quad (2)$$

where q_{Diss} and $q_{i,Lang}$ are the equilibrium boron uptakes due to absorption/partitioning in the membrane and sorption to Langmuir site *i*, respectively (mmol/g dry polymer), *n* is the number of Langmuir sites, K_{Diss} is the linear partition coefficient for boron absorption in the polymer (L solution/g dry polymer), $K_{i,Lang}$ is the Langmuir affinity constant of site *i* (L solution/mmol), and $q_{i,max}$ is the maximum Langmuir sorption capacity of site *i* (mmol/g dry polymer). The dual mode sorption model is commonly used to describe gas sorption in polymers at temperatures below their glass transition temperatures, as it considers linear partitioning in the polymer as well as sorption in the unrelaxed volume of the glass [51]. In the hydrated PGGE and PGGE-NMDG membranes, several moieties including epoxide and NMDG groups provide selective binding sites for boron that can be described using the Langmuir isotherm model, and the linear portion of the isotherm is attributed to boron dissolved in the membrane via other interactions (*e.g.*, electrostatic, van der Waals). The linear isotherm model assumes that boron affinity for the dissolved membrane phase does not change as a function of aqueous boron concentration.

Boron sorption in PGGE was modeled using a single-site Langmuir model to account for all potential moieties (*i.e.*, sites) in PGGE that specifically interact with boron (*e.g.*, epoxide, ether, amine, and hydroxyl groups) and a linear model to account for partitioning into the membrane phase. The dual mode model for boron sorption in PGGE-NMDG contained two types of Langmuir sites (with different affinities and capacities) to represent specific interactions between

boron and PGGE sites and chelation of boron by NMDG. To fit the boron sorption isotherm model for PGGE-NMDG, the Langmuir affinity parameter, K_{Lang}, for PGGE sites was fixed to the value determined for the PGGE control membrane, as the interactions between boron and PGGE sites were not expected to change significantly upon functionalization of PGGE with NMDG. The linear partition coefficient, K_{Diss}, for the isotherm model of boron sorption in PGGE-NMDG was constrained to be equal to or greater than the value obtained for the PGGE control membrane because PGGE-NMDG had a higher water uptake than PGGE. Also, the maximum Langmuir capacity, q_{max}, of PGGE sites in PGGE-NMDG was constrained to be less than or equal to the value for the PGGE control membrane, as the conversion of epoxide groups to NMDG was not expected to increase the number of PGGE sites in the PGGE-NMDG membrane relative to the PGGE control membrane. The resulting four-parameter dual mode isotherm model was shown to provide a better fit to the experimental boron sorption data for PGGE-NMDG relative to several other models based on the Akaike information criterion (AIC), which accounts for the ability of a model with more parameters to provide a better fit based on common error minimization/weighting procedures. Additional information on the sorption isotherm models and AIC analysis is provided in Section S3 of the Supplementary Materials.

Equilibrium sorption data for the commercial Amberlite IRA743 resin were fit to a single-site Langmuir isotherm (*i.e.*, only the second term in equation 2 with n=1). All fitting coefficients were determined in Matlab (MathWorks, Natick, MA) using a nonlinear least squares regression fitting technique within the Optimization Toolbox.

2.7. Sorption-desorption rate studies

To investigate transient transport of boron within PGGE and PGGE-NMDG membranes, sorption and desorption rate experiments were performed on pristine and regenerated membranes in well-mixed stirred solutions of finite volume. Dry membrane samples were weighed and hydrated in background solution matrices (*i.e.*, 10 mM HEPES, pH 7.0) for 24 h, and wet masses were recorded prior to rate experiments. Then, hydrated membrane samples were placed in solutions containing 10 mM boric acid and 10 mM HEPES (pH 7.0), and 100 µL aliquots were collected over 48 h to track the uptake of boron into the membranes. After sorption equilibrium was attained, the membranes were placed in 10 mM HEPES (pH 7.0) for desorption rate experiments, and 100 µL aliquots were collected over 48 h to track boron release from the membranes. A second desorption equilibrium stage was performed to investigate sorption hysteresis via comparison of boron uptake measurements in desorption equilibrium experiments and in equilibrium sorption isotherms. Then, this process was repeated on the same membranes. At the end of the second set of sorption-desorption rate experiments, the membrane samples were dried in a vacuum oven overnight and microwave digested to determine the amount of boron in the membranes following the final desorption stage.

Transient transport of boron in PGGE and PGGE-NMDG membranes was described using a one dimensional model for Fickian diffusion in a plane sheet from a stirred solution of limited volume [52]. Using this approach, apparent average diffusion coefficients of boron in PGGE and PGGE-NMDG membranes were determined for each sorption and desorption rate experiment using a nonlinear curve fitting technique in Matlab. The apparent average diffusion coefficients were normalized to the polymer phase using a series resistance model per a previously reported method [47]. More information on the modeling approach can be found in Section S5 of the Supplementary Materials.

2.8. Acid regeneration experiments

To assess the acid regeneration potential of PGGE and PGGE-NMDG membranes, four cycles of boron sorption in 10 mM HEPES and desorption in hydrochloric acid were performed. First, dry samples of PGGE and PGGE-NMDG membranes were weighed and hydrated in 10 mM HEPES (pH 7.0) for 24 h. Then, membranes were placed in aqueous solutions containing 10 mM boric acid and 10 mM HEPES (pH 7.0) and shaken for 48 h to ensure sorption equilibrium. Following sorption equilibrium, the membranes were placed in 0.1 M (cycle 1) or 1.0 M (cycles 2–4) hydrochloric acid to desorb the boron, and 100 µL aliquots of the solutions were collected periodically to investigate the boron desorption rates of the materials in acid (*cf*., Section 2.7). After apparent desorption equilibrium was reached, the membranes were placed in 10 mM HEPES (pH 7.0) for 24 h and the sorption/desorption cycle was repeated. After four cycles of acid regeneration, the membranes were microwave digested to assess if any boron remained in the membranes.

3. Results and Discussion

3.1. Cross-linked PGGE and PGGE-NMDG membranes

Polyether materials – typically, poly(ethylene oxide)-based – have seen widespread use in gas separations [53–56], drug delivery [57], and polymer electrolytes [58] due to their compositional versatility and the widespread availability of monomers. This study leveraged the versatility of PAGE to create crosslinked membranes with tunable physical properties that could be functionalized with ligands such as NMDG. With PGGE, epoxy/amine coupling was employed for crosslinking PGGE with 1,4-diaminobutane and for adding functional groups to

the backbone of the network in a single step (*cf.*, Figure 1). NMDG contains a secondary amine that participates in simultaneous epoxy/amine crosslinking/functionalization. *In situ* FTIR measurements show that the formation of C–N bonds involved in the simultaneous cross-linking and NMDG-functionalization of PGGE reaches completion after approximately 6 h (Figure S4) [59], resulting in the functionalized, crosslinked membrane. Water uptake in the composite PGGE-NMDG membranes is within the range of typical polymer membranes (*ca.* 0.35–0.70 g water/g dry polymer) (*cf.*, Table 1) [60], and the higher water uptake in PGGE-NMDG relative to the PGGE control membrane is attributed to the hydrophilicity of the NMDG functional group. Crosslinker density was held constant at 20 mol percent in the synthesized membranes; however, due to the impact of crosslinker density on water permeability and water/salt selectivity in hydrogel membranes [61], the optimization of crosslinker density for the PGGE and PGGE-NMDG membranes could be investigated in the future to maximize boron selectivity in these ligand-functionalized membranes.

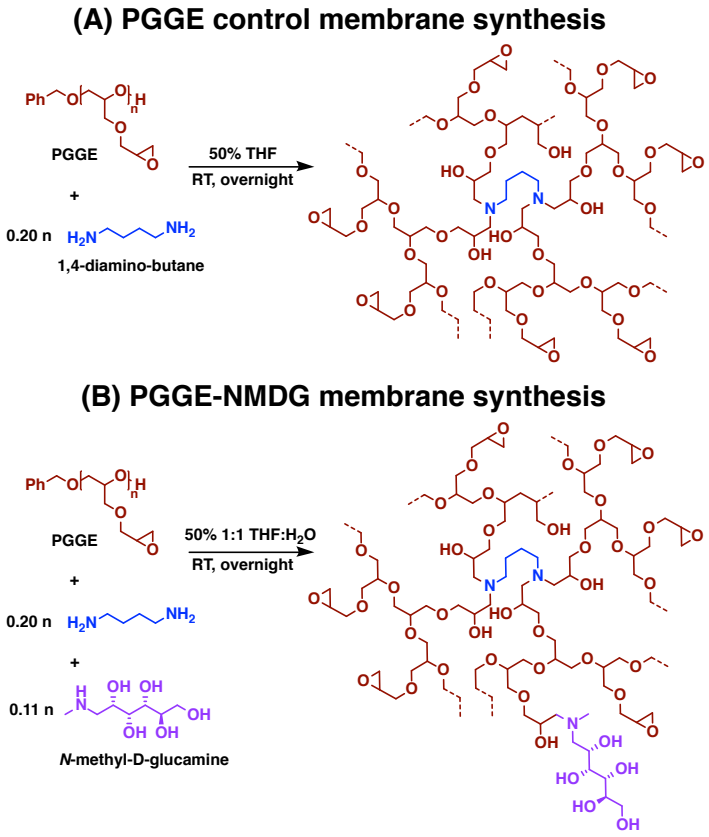

338

339 **Figure 1.** General scheme for the synthesis of: (A) PGGE and (B) PGGE-NMDG membranes.

340

341 **Table 1.** Material properties of PGGE and PGGE-NMDG membranes.

Property	**PGGE**	**PGGE-NMDG**
Water uptake in composite membrane (g/g)	0.372 ± 0.013	0.442 ± 0.037
Water uptake in dense polymer (g/g)	0.527 ± 0.034	0.684 ± 0.034
Water volume fraction in hydrated polymer (-)	0.374 ± 0.013	0.430 ± 0.007

342

343 *3.2. Equilibrium boron sorption*

344 As shown in Figure 2, boron sorption isotherms of PGGE and PGGE-NMDG membranes

345 exhibited dual mode sorption behavior, while the commercial BSR followed a Langmuir

346 isotherm typical of macroreticular resins, including previously-studied BSRs [21,62]. All three
347 materials exhibited Langmuir sorption behavior at low solution-phase boron concentrations,
348 presumably due to specific interactions between boron and functional groups in the
349 membranes/resin. PGGE membranes provide binding sites that can be described with a single-
350 site Langmuir model that assumes all sites are equivalent, while PGGE-NMDG membranes
351 contain two Langmuir sites due to the additional presence of NMDG in the membranes. The two-
352 site Langmuir model assumes sorption to the two binding sites are independent. Linear boron
353 sorption behavior in PGGE and PGGE-NMDG describes boron absorption/partitioning in the
354 membranes in direct proportion to the solution-phase boron concentration due to intermolecular
355 interactions (*e.g.*, electrostatic, van der Waals).
356

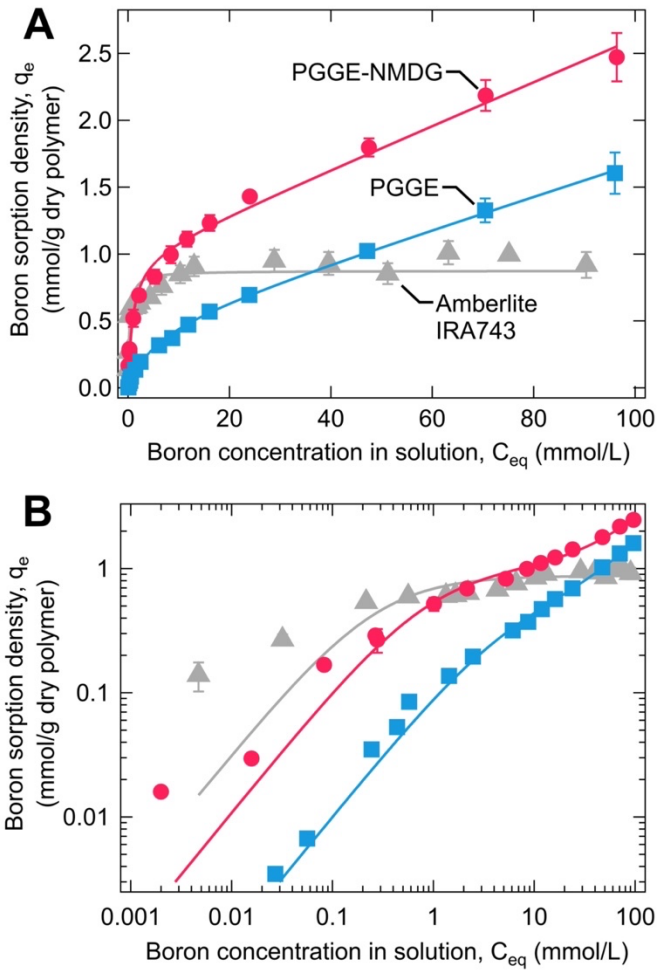

Figure 2. Boron uptake in PGGE (squares) and PGGE-NMDG (circles) membranes followed dual mode sorption isotherms, while the commercial BSR (triangles) exhibited Langmuir isotherm behavior. The same data are plotted on: (A) linear and (B) log-log scales to show trends over a range of concentrations. All experimental data were performed in 10 mM HEPES (pH 7.0) buffer and equilibrated for 48 hours. Error bars represent standard deviations of measurements on at least three membrane/resin samples and lines represent the fit of the isotherm models to the data.

366 The specific (*i.e.*, Langmuir) interactions between boron and the membranes dominated at
367 low aqueous boric acid concentrations relevant to water treatment applications such as seawater
368 desalination, where influent boron concentrations are 0.5 mmol/L [9]. The sorption capacity,
369 q_{max}, of NMDG sites in PGGE-NMDG was lower than that of the commercial BSR (*cf.*, Table 2),
370 indicating that the average binding stoichiometry of the boron-NMDG complexes in PGGE-
371 NMDG was less than one since the synthesis conditions were designed assuming 1:1 complexes
372 to match the boron sorption capacity of the commercial BSR. As shown in Table 2, the Langmuir
373 affinity coefficient, K_{Lang}, of PGGE-NMDG was also lower than that of the commercial BSR,
374 which may be due to the different nature of the materials (*i.e.*, hydrated polyether membrane
375 versus macroreticular resin with a hydrophobic polystyrene backbone). The sorption capacity
376 and Langmuir affinity coefficient of NMDG sites in PGGE-NMDG are comparable to the values
377 for similar NMDG-functionalized materials reported in literature (*cf.*, Table S3). Interactions at
378 the water-membrane/resin interface influence boron sorption affinity and mechanisms. For
379 example, electrostatic interactions between borate and residual metal cations on BSR surfaces
380 have been shown to contribute to boron uptake in NMDG-functionalized resins [63]. The
381 isotherm models for Amberlite IRA743 and PGGE-NMDG underpredicted experimental
382 sorption measurements at aqueous boron concentrations below 0.1 mmol/L (*cf.*, Figure 2),
383 suggesting that the Langmuir and dual mode isotherm models may not fully capture the
384 interactions between boron and the membranes/resin at low equilibrium solution-phase boron
385 concentrations.
386

Table 2. Fitted isotherm parameters for boron sorption in the membranes and BSR.

Sample	Absorption	PGGE sites		NMDG sites	
	K_{Diss} (L/g)	K_{Lang} (L/mmol)	q_{max} (mmol/g)	K_{Lang} (L/mmol)	q_{max} (mmol/g)
PGGE	0.012 ± 0.0004[a]	0.18 ± 0.03	0.49 ± 0.03	-	-
PGGE-NMDG	0.015 ± 0.0006	0.18[b]	0.49 ± 0.14	2.5 ± 0.76	0.62 ± 0.10
Amberlite IRA743	-	-	-	3.7 ± 1.3	0.88 ± 0.04

[a]Plus/minus values represent standard deviations of fitted values.

[b]The value of K_{Lang} of PGGE sites in PGGE-NMDG was fixed to the value obtained for the PGGE control membrane, and the remaining four parameters were fit using a nonlinear least squares regression. Details of the fitting process are presented in Section S3 of the Supplementary Materials.

The PGGE control membrane also exhibited some affinity for boron, suggesting that the epoxide groups in PGGE, the hydroxyl groups formed upon epoxide ring opening, the amine groups in the crosslinker, and/or the backbone polyether interact with boron, although to a lesser extent than the NMDG ligand. Possible interactions that contribute to the observed behavior include Lewis pairing of boron and oxygen heteroatoms and hydrogen bonding between hydroxyl groups in boric acid and oxygen- and nitrogen-containing moieties in PGGE. Boric acid, as well as various boranes and boronic acids, have been used as hydrogen bond donors and Lewis acid catalysts during epoxide ring opening for applications including carbon dioxide conversion to cyclic carbonates [64–68]. Moreover, recent work by Kim *et al.* [69] showed boric

acid suppresses curing of epoxy resins; the authors attributed this behavior to hydrogen bonding of hydroxyl groups in boric acid and oxygen in epoxide groups. Bernstein *et al.* [26] used an epoxide surface graft to increase boric acid rejection of a commercial RO membrane and attributed the observed increase in rejection to caulking/sealing of defects by the adhesion of epoxides through reaction with amine groups in the polyamide RO membranes. The boron sorption isotherm of the PGGE membrane suggests that specific interactions between boron and epoxide also influence boron rejection during RO using epoxide-grafted membranes.

Linear partitioning of boron in PGGE and PGGE-NMDG membranes contributes significant boron uptake at aqueous boric acid concentrations above 10 mmol/L. Meanwhile, the hydrophobic, polystyrene-based Amberlite IRA743 resin had no appreciable absorption of boron despite a comparable water uptake of the resin (0.48–0.54 g water/g dry polymer) relative to PGGE and PGGE-NMDG (0.53–0.68 g water/g dry polymer) [45]. Since boric acid can hydrogen bond with water [70], the higher water uptake of the PGGE-NMDG membrane likely contributed more boron absorption (*i.e.*, a higher slope of the linear portion of the curve in Figure 2) relative to the PGGE control membrane. Polyborates form in solution when total boron concentrations are greater than 25 mmol/L [71], but the constant slopes of the linear isotherms at aqueous boron concentrations above 25 mmol/L suggest that the formation of polyborates did not have a direct impact on boron sorption in studied membranes and BSR at equilibrium solution concentrations up to 100 mmol/L.

Using measured values of dry polymer mass and swollen volumes of PGGE and PGGE-NMDG membranes, conversion of K_{Diss} values presented in Table 2 to volumetric partition coefficients – defined as the ratio of solute concentration in the swollen membrane to the concentration in the external solution – yield values of 6.8±0.65 and 6.5±0.35 L external

solution/L swollen membrane for PGGE and PGGE-NMDG, respectively. The partition coefficient of dehydrated boric acid in a commercial polyamide active layer has been reported as 0.45 L solution/L swollen membrane [72]. The large linear partition coefficients of boron in the polyether membranes indicate that the membranes provide a thermodynamically favorable environment for boron relative to the aqueous solution (*i.e.*, the interactions between boron and neighboring molecules in the dissolved membrane phase are more favorable than that of boron and water). Hydrogen bonding between boric acid molecules absorbed in the polymer matrix and boron bound to PGGE and/or NMDG sites is a possible reason for the large partition coefficient of boron from the bulk solution to the hydrated membranes, as hydrogen-bonded structures containing boric acid have previously been found in aqueous and polymer systems [73,74]. Hydrogen bonding has been found to contribute to high sorption (3–8 L external solution/L swollen membrane) of arsenious acid ($As(OH)_3$) in polyamide membranes [75]. In the context of the solution-diffusion model, the high partition coefficient of boron in PGGE and PGGE-NMDG membranes would increase boron permeation by a selective membrane layer unless boron diffusion is significantly slowed by interactions between boron and the polymer.

3.3. Ex situ ATR-FTIR investigation of boron-NMDG interactions

Figure 3 presents *ex situ* ATR-FTIR spectra of dried PGGE-NMDG membranes equilibrated at several solution-phase boron concentrations following subtraction of the spectra of the pristine PGGE-NMDG membrane (*i.e.*, the membrane with zero boron sorbed). The raw ATR-FTIR spectra prior to subtraction of the pristine membrane are provided in Figure S10. At all tested solution-phase boron concentrations, peaks at approximately 950 cm^{-1} are noted, representative of the asymmetric B–O stretch of tetrahedral borate anions (*cf.*, Figure S9) [76]. ATR-FTIR

spectral changes coming from the asymmetric stretch of boric acid, which occurs in the range 1300–1500 cm^{-1} [76], were not as significant as the changes from borate in the PGGE-NMDG spectra, suggesting that boron interacted with the NMDG groups as tetrahedral borate anions despite boric acid being the dominant species of boron in solution. Peak *et al.* [76] suggested that the speciation of boron at the surface of mineral oxides is generally quite different than that of the bulk solution, and Yoshimura *et al.* [77] showed the amino group in NMDG promotes formation of borate-NMDG complexes when Amberlite IRA743 resin is equilibrated with neutral solutions of boric acid. FTIR peaks from B–O–H in plane (1150 cm^{-1}) and out of plane (800 cm^{-1}) bending are apparent when the boron concentration in the external solution was 10 and 100 mmol/L (*cf.*, Figure 3), presumably due to higher boron absorption in PGGE-NMDG at increased solution-phase boron concentrations. The subtracted ATR-FTIR spectra of the PGGE-NMDG membranes also feature negative absorbance peaks at 1350 and 1600 cm^{-1}, which are attributed to the deprotonation of hydroxyl groups and the loss of water/carbonate following boron sorption, respectively [76,78]. The PGGE control membranes showed no significant boron-induced FTIR peaks except those from B–O–H bending at external boron concentrations of 10 and 100 mmol/L (*cf.*, Figure S10).

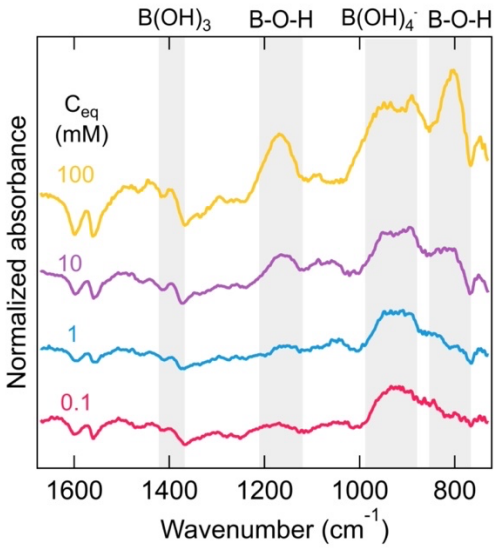

Figure 3. ATR-FTIR spectra of PGGE-NMDG membranes equilibrated with several aqueous concentrations of boric acid (C_{eq}) following subtraction of the spectra of the pristine PGGE-NMDG membrane (*i.e.*, the membrane equilibrated at C_{eq}=0 mmol/L). The appearance of a peak at approximately 950 cm^{-1} is indicative of borate-NMDG interactions that increase in intensity and variability (*i.e.*, peak width) as aqueous boron concentration is increased. Peaks from B–O–H in plane (1150 cm^{-1}) and out of plane (800 cm^{-1}) bending also emerge with increasing boron concentration, but changes in the boric acid-induced peaks (1400 cm^{-1}) are less significant.

As boron loading increased in PGGE-NMDG, the relative intensity and width of the peak from tetrahedral borate increased, with the most significant change occurring between 10 and 100 mmol/L boron in the external solution containing boric acid (*cf.*, Table S4). This trend implies the formation of borate-NMDG complexes with a range of molecular configurations at increased solution phase concentrations. Based on boron sorption isotherms in Figure 2, boron uptake capacity in PGGE-NMDG does not seem to be significantly impacted by conformational changes of the boron-NMDG complexes, yet the formation of different boron-NMDG complexes

at different concentrations of boric acid could be the reason for the poor agreement between experimental sorption data and the Langmuir and dual mode isotherm models of Amberlite IRA743 and PGGE-NMDG, respectively, at aqueous boron concentrations below 0.1 mmol/L.

Boron can form several monochelate and bischelate complexes with NMDG [63,77,79,80], and the formation of specific complexes influences both boron uptake capacity and boron mobility within the material. Assuming that all of the NMDG in the polymerization mixture was incorporated into PGGE-NMDG membranes, the average binding stoichiometry of boron-NMDG complexes in PGGE-NMDG – defined as the ratio of the maximum Langmuir sorption capacity, q_{max}, of the NMDG sites over the NMDG loading in PGGE-NMDG – was 0.63 mol B/mol NMDG. Ratios in the range 0.36–2.1 mol B/mol NMDG have been reported in literature for several NMDG-functionalized materials (*cf.*, Table S3). Previous studies using ^{11}B NMR suggested the preferential formation of bischelate borate-NMDG complexes in BSRs [21,63,77,80], which would yield a binding stoichiometry of 0.5. Density-functional theory simulations of boron complexation with NMDG in an aqueous system by Ide and Hirayama [79] showed that two NMDG groups can complex with two borate molecules, yielding a binding stoichiometry of one. Monochelate complexes (*e.g.*, bidentate, tetradentate) would also yield a binding stoichiometry of one. Yoshimura *et al.* [77] suggested the preferential formation of the tetradentate borate-NMDG complex in a crosslinked polymer due to dehydration caused by the lower activity of water in the resin phase, but in hydrated systems, tetradentate borate-NMDG complexes have been considered thermodynamically unfavorable due to ring strain [79]. Additional factors including binding strength of individual complexes and accessibility of binding sites also influence the distribution of boron-NMDG complexes in BSRs and polyol-functionalized membranes. Based on the boron-NMDG binding stoichiometry and ATR-FTIR

data, the distribution of boron-NMDG complexes in PGGE-NMDG membranes likely included a combination of monochelate and bischelate complexes that varied as a function of boron uptake.

3.4. Boron sorption-desorption rate studies

As shown in Figure 4, boron sorption in PGGE and PGGE-NMDG membranes was partially reversible through two cycles of sorption-desorption in 10 mM HEPES (pH 7.0) buffer, and microwave digestion of the membranes at the end of the second cycle confirmed the presence of residual boron in both membranes. The initial aqueous boron concentration used in sorption experiments (10 mM) was chosen to capture the upper-limit of the Langmuir-dominated portion of the sorption isotherms. In turn, the transient data collected during the sorption-desorption rate experiments provide fundamental insight into boron diffusion in the membranes when boron-ligand interactions are significant.

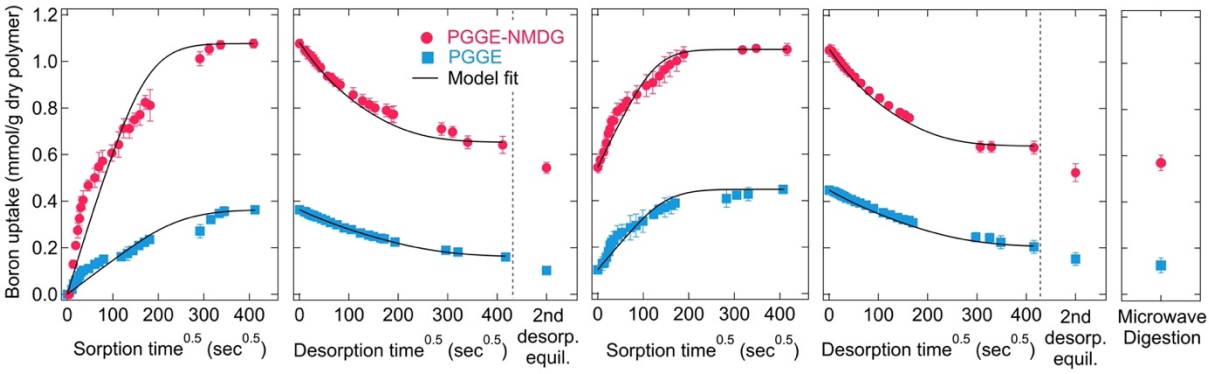

Figure 4. Transient sorption and desorption of boron in PGGE (squares) and PGGE-NMDG (circles) membranes. Lines represent the fits of a one-dimensional Fickian diffusion model without sorption explicitly included, as described in Section S5 of the Supplementary Materials. Sorption experiments were performed in 10 mM boric acid solutions in 10 mM HEPES (pH 7.0), while desorption experiments were performed in 10 mM HEPES (pH 7.0) with no boric acid.

The one-dimensional Fickian diffusion model predicts a linear relationship between boron uptake in the membranes and the square root of time, as shown in Figure 4, but the experimental boron uptake values obtained in sorption and desorption rate experiments do not exhibit the same behavior. In fact, two-stage sorption is observed for boron uptake in PGGE and PGGE-NMDG membranes during sorption-desorption rate experiments, indicating that boron transport in the membranes is not strictly controlled by a single diffusion process. Whereas linear sorption would be captured in a Fickian diffusion model for linear, local equilibrium and reflected in an apparent diffusion coefficient for transport in the membrane, that approach was not able to describe the two-stage sorption behavior observed in PGGE and PGGE-NMDG membranes.

The two-stage sorption behavior was not caused by the composite membrane structure (*i.e.*, the dense top layer and supported composite layer). A control experiment was conducted by monitoring phenylboronic acid uptake in a composite membrane having XLPEGDA impregnated in a porous polypropylene support membrane. Phenylboronic acid was chosen for this investigation because it exhibits a high partition coefficient in XLPEGDA relative to boric acid, so changes in external solution boron concentrations changed significantly during sorption rate experiments and thus were detectable via ICP-OES. XLPEGDA was chosen as the model membrane because XLPEGDA was previously used to investigate the impact of polypropylene support membranes on salt sorption and permeation in composite membrane structures [47]. The results of this control experiment are set forth in Section S3 of the Supplementary Materials. Phenylboronic acid uptake in the composite XLPEGDA membrane followed the behavior predicted by a one-dimensional Fickian diffusion model that incorporates linear, local-equilibrium partitioning, and the data did not exhibit the two-stage behavior shown in the

sorption experiments in Figure 4. Thus, the two-stage behavior observed during boron sorption rate experiments is ascribed to interactions of boron with PGGE and PGGE-NMDG.

Two-stage sorption has been attributed to the initial filling of easily-accessible sorption sites followed by diffusion and sorption to remaining sites, as previously reported in ion exchange resins with bidisperse pore structures [81] and in glassy polymers undergoing polymer relaxation during solute uptake/diffusion [82–84]. In PGGE and PGGE-NMDG membranes, conformational changes in the polymer network following specific solute/membrane interactions such as hydrogen bonding between boron and PGGE sites and/or the formation of boron-NMDG complexes could retard boron transport and contribute to the observed two-stage sorption behavior.

While transport of boron in PGGE and PGGE-NMDG membranes was not completely diffusion controlled, the calculation of apparent average Fickian diffusion coefficients allowed further investigation of the important mechanisms that control boron transport in the membranes. As shown in Table 3, the apparent average diffusion coefficients of boron in PGGE and PGGE-NMDG are low relative to diffusion of reference solutes (*i.e.*, methanol and NaCl) in XLPEGDA membranes with similar water uptake [85,86], supporting the hypothesis that sorptive boron-membrane interactions control boron transport in PGGE and PGGE-NMDG membranes. The apparent diffusion coefficients of boron in PGGE and PGGE-NMDG are only 0.9-5.9% of the values predicted using the Mackie-Meares model (Table S5), which accounts for polymer chain obstruction (*i.e.*, tortuosity) effects on solute diffusivity in polymer membranes [87]. Possibly, hydrogen bonding and Lewis pairing of boric acid with other boric acid molecules and polymer functional groups in PGGE and PGGE-NMDG membranes, which were hypothesized to

564 contribute significantly to boron sorption in Section 3.2, limits diffusion of boron in the
565 membranes.
566

567 **Table 3.** Apparent boron diffusion coefficients in PGGE and PGGE-NMDG membranes, as well
568 as reference solute diffusion coefficients in cross-linked poly(ethylene glycol) diacrylate
569 (XLPEGDA) taken from literature [85,86].

Experiment[a]	D_{app}[b] (10^{-8} cm^2/s)	
	PGGE	**PGGE-NMDG**
S-1	1.9 ± 0.32	2.8 ± 0.39
D-1	0.99 ± 0.16	1.1 ± 0.10
S-2	5.0 ± 1.2	5.2 ± 1.5
D-2	0.98 ± 0.03	1.1 ± 0.09
1 mol/L methanol in XLPEGDA	235[c]	
1 mol/L NaCl in XLPEGDA	125 ± 50	

[a]S=sorption; D=desorption; 1=pristine membrane; 2=regenerated membrane. Entries below the dividing line were taken from literature for solutes in XLPEGDA membranes with water uptake of approximately 0.7 g water/g dry polymer, similar to the water uptake in PGGE-NMDG (*cf.*, Table 1).

[b]Apparent diffusion coefficients were determined using a one-dimensional Fickian diffusion model without sorption explicitly included, as described in Section S5 of the Supplementary Materials. The sorption-desorption rate data presented in Figure 4 were fit to the model to extract apparent diffusion coefficients. Plus/minus represent the standard deviation of values among three membrane samples.

[c]No uncertainty was reported for this value.

570

571 The apparent diffusion coefficient of boron in PGGE-NMDG is larger than that in PGGE
572 during the sorption rate experiments using the pristine membranes (*i.e.*, experiment S-1 in Table
573 3), but insignificant differences in apparent average boron diffusion coefficients are noted
574 between the two membranes in all other experiments. Boron diffusion appeared slower in the
575 pristine membranes relative to the regenerated membranes, possibly due to the filling of
576 Langmuir sites. The higher apparent diffusion coefficient of boron in the pristine PGGE-NMDG
577 membrane relative to the pristine PGGE membrane is attributed to the boron affinity for the
578 NMDG sites and the higher water uptake of PGGE-NMDG relative to the PGGE control
579 membrane. However, when the Langmuir sites were (partially) filled, the boron-NMDG
580 interactions were less significant, and boron diffusion was likely controlled by the boron-PGGE
581 interactions (*e.g.*, hydrogen bonding to epoxide groups).
582 Desorption rate experiments yielded lower apparent diffusion coefficients than sorption rate
583 experiments for both membranes, which may be caused by polymer conformational changes at
584 sorption equilibrium to favor different boron-PGGE and boron-NMDG complexes with varying
585 levels and rates of reversibility that lead to desorption resistance and hysteresis, respectively.
586 This phenomenon has been noted for solute sorption in organic matter of soil/sediment systems
587 and other materials relevant to water treatment [88–90]. Indeed, sorption/desorption hysteresis
588 was noted for boron uptake in the PGGE-NMDG membrane (*cf.*, Figure S7), and deviations
589 among the sorption isotherms and the desorption rate equilibrium data for both membranes (*cf.*,
590 Figure S8) confirm a significant role of desorption resistance during desorption rate experiments.
591 Previous researchers have modeled diffusion of water-soluble drugs (*e.g.*, riboflavin,
592 acetazolamide) in hydrogels where solute-specific binding is significant; these studies used a
593 local sorption equilibrium model based on linear partitioning to polymer sorption sites to

describe the significant (*i.e.*, orders of magnitude) decrease in apparent diffusion coefficients due to specific interactions between drugs and hydrogel-polymer chains [91]. The observed hysteresis during desorption rate experiments limited the applicability of a local Langmuir sorption equilibrium model to accurately describe the impact of sorptive interactions on boron transport but warrants future investigation. Local sorption equilibrium models assume that sorptive interactions occur on much faster time scales than diffusion; other models have considered diffusion-immobilization processes for cases where sorption and diffusion proceed at comparable rates [92]. Future research in this space could establish fundamental structure/property rules for solute selectivity in ligand-functionalized membranes and lead to the design of new materials with desired properties (*e.g.*, water uptake, ligand density) for achieving transport or removal of target solutes during membrane filtration.

3.5. Membrane regeneration

Affinity-based separations using adsorbents and ion exchange resins rely on regeneration of the material for continued reuse, and the development of ligand functionalized membranes must adapt similar approaches if removal is achieved through a capture-and-release mechanism. While boron sorption in the membranes was partially reversible in 10 mM HEPES solutions, the regeneration of the membranes in acid would be required for full-scale applications because acid regeneration is generally faster than regeneration in neutral solution, thus minimizing downtime and limiting the volume of the generated waste stream. At acidic conditions (*i.e.*, low pH), borate-polyol complexes are hydrolyzed to release boric acid from the polyol complex (*cf.*, Figure S13) [93]. As shown in Figure 5, PGGE and PGGE-NMDG membranes retained their boron uptake capacities through four cycles of batch sorption and acid regeneration experiments.

Microwave digestion of the membranes at the end of the fourth cycle showed no residual boron in the materials. This result confirms the reversibility of the boron-PGGE and boron-NMDG interactions in the membranes using acid. Indeed, vicinal hydroxyl groups generally exhibit good pH-reversibility for borate complexes, as highlighted by previous studies on polyol-functionalized adsorbents [19–21] and the use of dynamic covalent boronic esters in hydraulic fracturing fluids [94,95], molecular sensing [96], and several biomedical applications [97,98]. The stability constants of monochelate and bischelate borate-NMDG complexes in aqueous solution have been reported to be $10^{4.9}$ M and $10^{6.3}$ M, respectively [77]. These values are within the range proposed by Millner [99] of stability constants for protein-ligand interactions employed in membrane chromatography such that the binding is both selective and reversible (10^4–10^8 M). While the stability constant of the boron-epoxide interaction is not known, the lower binding affinity, K_{Lang}, of boron to PGGE relative to the NMDG-functionalized materials (*cf.*, Table 2) support the findings that this interaction is reversible via acid regeneration.

In 1.0 M HCl, complete boron desorption from the membranes occurred in less than 1 h, and desorption occurred within 2 h in 0.1 M HCl. The rate of boron release during acid desorption experiments exhibited linear behavior versus the square root of time, suggesting Fickian diffusion behavior (Figure S12). In HEPES, the partial desorption of boron from the membranes to a new equilibrium position occurred over >24 hours (*cf.*, Figure 4). Acids of higher strength could be used to further increase desorption rates, and Meng *et al.* [20] showed 4 M HCl enabled complete desorption of boron from a complexing membrane in a similar batch system within 15 minutes. Adapting the approach of the IonPac® boron-selective ion exchange column [100], regeneration could also be possible through the passage of aqueous polyol species that exhibit higher binding affinities than the immobilized NMDG groups in PGGE-NMDG membranes. The

optimization of such process design considerations in a flow regime presents interesting opportunities for research needed before incorporation of NMDG membranes in full-scale treatment trains. No significant degradation of the polyether membranes was noted after four cycles of acid regeneration. Ring opening of epoxides in PGGE and PGGE-NMDG was not noted following aqueous washing during polymer synthesis (per ^{1}H NMR results presented in Figure S2) or during acid regeneration experiments (per constant boron uptake through four regeneration cycles), but hydrolysis of the polyether materials over extended use could influence membrane stability in full-scale operations [101].

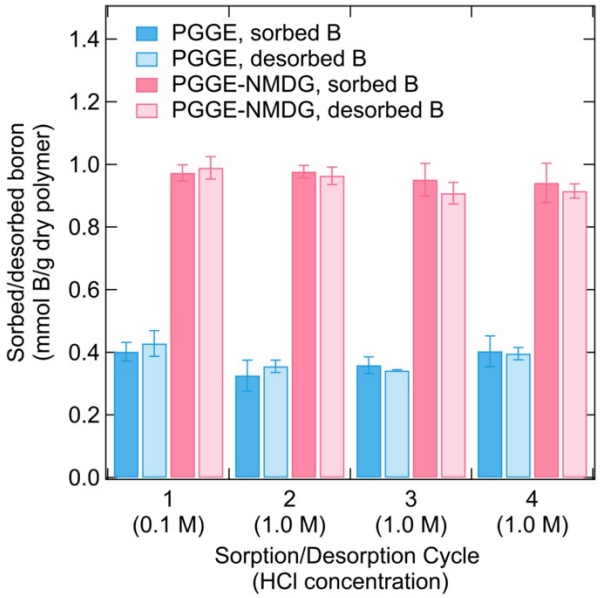

Figure 5. Boron sorption in PGGE and PGGE-NMDG membranes was reversible through four cycles of acid desorption. Sorption equilibrium measurements were performed over 48 h in 10 mM boric acid and 10 mM HEPES (pH 7.0), while desorption experiments were performed in 0.1 M (cycle 1) or 1.0 M (cycles 2-4) hydrochloric acid (HCl) until equilibrium was reached (within 2 h, see Figure S12).

3.6. Implications: Full-scale regeneration times

The membranes synthesized and characterized in this study exhibit high affinity for boric acid and excellent regeneration potential during batch experiments, but in a real-world setting, the membranes would be used in continuous flow. PGGE and NMDG Langmuir sites in PGGE-NMDG membranes provide boron removal through a capture-and-release mechanism. Low saturation capacities are a primary challenge in adapting chelating membranes instead of high surface area resins in water treatment [32], so membranes must exhibit sufficient capacities such that regeneration is only needed periodically. To assess the potential for NMDG functionalized membranes to remove boron during full scale water treatment operations through a capture-and-release mechanism, the saturation time of NMDG sites in dense, RO membranes was estimated based on the boron sorption isotherm of the NMDG membranes developed herein (*cf.*, Figure 2) and the operating conditions of the Ashkelon desalination plant in Israel. Additional information on these calculations can be found in Section S7 of the Supplementary Materials.

By assuming that NMDG-functionalized RO membranes equilibrate with 0.4 mg B/L (*i.e.*, the desired effluent concentration) during permeation of a feed water containing 4 mg B/L (*i.e.*, 90% removal), regeneration of NMDG sites is needed after less than one minute of operation, with each of the membrane elements having the capacity to capture just two mg of boron. This finding suggests that RO membrane layers are not viable for removal by capture-and-release alone due to a limited number of binding sites in the ultrathin membranes. To this end, the microporous support structure of RO membranes can be functionalized to provide additional sites, and by using the boron sorption isotherm of the NMDG-grafted polysulfone membranes reported in Du *et al*. [35] with the typical properties of RO support structures (*cf.*, Table S6), the saturation time of the membranes could be extended to 0.7 h. Not considering the

time required for regeneration, which would need to be on the order of minutes to make this process feasible, this approach still requires 30 regeneration cycles a day, but it assumes that all of boron in the feed water is removed by the NMDG sites.

Current seawater RO membranes reject up to 90% of influent boron concentrations at neutral pH, while novel membranes can achieve higher rejection (>95%) [13]. Removal of 90% of influent boron is necessary for single-pass boron removal (assuming influent and product boron concentrations at the Ashkelon plant of 4 and 0.4 mg/L, respectively), so a conservative estimate of 80% removal of influent boron by a selective RO membrane layer was used to investigate the saturation time of NMDG sites in the porous support. This calculation shows that regeneration is needed every 6 h, suggesting that novel asymmetric membranes for high boron rejection could incorporate boron-rejecting selective layers and porous support layers with NMDG (or a similar boron-selective ligand) to act as an integrated polishing step. Perhaps, the epoxide sites in PGGE that were proposed to interact with boric acid in this study and in Bernstein *et al.* [26] could be considered in the design of boron rejecting selective layers. PGGE-NMDG membranes could also be investigated for other membrane processes such as electrodialysis, as recent work has shown promise for the capture of toxic metals during electrodialysis with adsorptive membranes [39].

While polyol-functionalized membranes provide a highly selective approach for removing boron from contaminated waters, feedwater chemistry must be considered in the design of processes that employ such materials. Clearly, feedwaters with high boron concentrations will saturate sorption sites faster and thus require frequent regeneration. Indeed, if the boron concentration of the influent water at the Ashkelon desalination plant increased from 4 mg B/L to 120 mg B/L (*i.e.*, the boron concentration of a produced water sample taken from the

Eagle Ford shale play [11]), the saturation time for sorption sites in the porous support (assuming 80% rejection by the selective RO layer) decreases from 6 h to 6 min. Additionally, since this fundamental study only investigated boron transport in the NMDG membranes when exposed to solutions of boric acid and HEPES, the selectivity of ligand-functionalized membranes should be investigated in complex solutions typical of unconventional waters (*e.g.*, high ionic strength).

4. Conclusions

A versatile membrane platform based on poly(glycidyl glycidyl ether) (PGGE) was functionalized with *N*-methyl-D-glucamine (NMDG) to provide selective removal of boric acid during water purification. PGGE and PGGE-NMDG membranes exhibited dual mode sorption isotherms for boric acid, presumably due to absorption of boron in the polymer matrix and additional specific interactions between boron and functional groups in the membranes. Specific interactions between boron and the membranes were well-described using a single-site and two-site Langmuir isotherm model for PGGE and PGGE-NMDG, respectively. PGGE interacted with boron via its epoxide, ether, and amine groups, and PGGE-NMDG also provided boron removal via chelation by NMDG. Experiments performed using buffered solutions of boric acid (pH 7.0) indicated that borate-NMDG complexes form in PGGE-NMDG membranes over all tested concentrations. Boron sorption in PGGE and PGGE-NMDG membranes was reversible over four cycles of acid regeneration without a significant loss of boron uptake capacity. Diffusion of boron in PGGE and PGGE-NMDG exhibited two-stage sorption behavior, which may result from specific solute/membrane interactions such as chelation by NMDG groups and hydrogen bonding with epoxide, ether, and amine groups. This study highlights several important properties of ligand-functionalized membranes that can be leveraged to enhance removal of challenging solutes such as boric acid during water reuse.

Acknowledgements

This work was supported as part of the Center for Materials for Water and Energy Systems (M-WET), an Energy Frontier Research Center funded by the U.S. Department of Energy, Office of Science, Basic Energy Sciences under Award #DE-SC0019272. The authors thank *General Electric Power and Water* for providing the porous polypropylene membranes used for membrane casting.

Author contribution statement

F.W.R. and B.J.P. made the materials and M.R.L. characterized them, and each of these authors wrote their respective portions of the manuscript. The remaining authors (L.E.K., N.A.L., D.F.L., and B.D.F.) supervised the research and provided critical feedback during data collection, analyses, and manuscript preparation.

References

[1] M.R. Landsman, R. Sujanani, S.H. Brodfuehrer, C.M. Cooper, A.G. Darr, R.J. Davis, K. Kim, S. Kum, L.K. Nalley, S.M. Nomaan, C.P. Oden, A. Paspureddi, K.K. Reimund, L.S.R. III, S. Yeo, D.F. Lawler, B.D. Freeman, L.E. Katz, Water treatment: Are membranes the panacea?, Annu. Rev. Chem. Biomol. Eng. 11 (2020) 1–27. https://doi.org/10.1017/CBO9781107415324.004.

[2] M. Elimelech, W.A. Phillip, The future of seawater desalination: Energy, technology, and the environment, Science. 333 (2011) 712–717. https://doi.org/10.1126/science.1200488.

[3] L.F. Greenlee, D.F. Lawler, B.D. Freeman, B. Marrot, P. Moulin, Reverse osmosis desalination: Water sources, technology, and today's challenges, Water Res. 43 (2009) 2317–2348. https://doi.org/10.1016/j.watres.2009.03.010.

[4] C.Y. Tang, Z. Yang, H. Guo, J.J. Wen, L.D. Nghiem, E. Cornelissen, Potable water reuse through advanced membrane technology, Environ. Sci. Technol. 52 (2018) 10215–10223. https://doi.org/10.1021/acs.est.8b00562.

[5] D.M. Warsinger, S. Chakraborty, E.W. Tow, M.H. Plumlee, C. Bellona, S. Loutatidou, L. Karimi, A.M. Mikelonis, A. Achilli, A. Ghassemi, L.P. Padhye, S.A. Snyder, S. Curcio, C.D. Vecitis, H.A. Arafat, J.H. Lienhard, A review of polymeric membranes and processes for potable water reuse, Prog. Polym. Sci. 81 (2018) 209–237. https://doi.org/10.1016/j.progpolymsci.2018.01.004.

[6] M. Brdar-Jokanović, Boron toxicity and deficiency in agricultural plants, Int. J. Mol. Sci. 21 (2020). https://doi.org/10.3390/ijms21041424.

[7] A.J. Kondash, J.H. Redmon, E. Lambertini, L. Feinstein, E. Weinthal, L. Cabrales, A. Vengosh, The impact of using low-saline oilfield produced water for irrigation on water

763 and soil quality in California, Sci. Total Environ. 733 (2020) 139392.
764 https://doi.org/10.1016/j.scitotenv.2020.139392.
765 [8] H. Miller, P. Trivedi, Y. Qiu, E.M. Sedlacko, C.P. Higgins, T. Borch, Food crop irrigation
766 with oil field-produced water suppresses plant immune response, Environ. Sci. Technol.
767 Lett. 6 (2019) 656–661. https://doi.org/10.1021/acs.estlett.9b00539.
768 [9] N. Hilal, G.J. Kim, C. Somerfield, Boron removal from saline water: A comprehensive
769 review, Desalination. 273 (2011) 23–35. https://doi.org/10.1016/j.desal.2010.05.012.
770 [10] Y. Jie, K. Goh, M. Kurihara, R. Wang, Seawater desalination by reverse osmosis: Current
771 development and future challenges in membrane fabrication – A review, J. Memb. Sci.
772 629 (2021) 119292. https://doi.org/10.1016/j.memsci.2021.119292.
773 [11] M.A. Sari, S. Chellam, Mechanisms of boron removal from hydraulic fracturing
774 wastewater by aluminum electrocoagulation, J. Colloid Interface Sci. 458 (2015) 103–111.
775 https://doi.org/10.1016/j.jcis.2015.07.035.
776 [12] B. Özyurt, Ş. Camcıoğlu, M. Fırtın, Ç. Ateş, H. Hapoglu, Boron removal from industrial
777 wastewaters by means of optimized sequential chemical precipitation and coagulation
778 processes, Desalin. Water Treat. 172 (2019) 292–300.
779 https://doi.org/10.5004/dwt.2019.24932.
780 [13] Y.P. Tang, L. Luo, Z. Thong, T.S. Chung, Recent advances in membrane materials and
781 technologies for boron removal, J. Memb. Sci. 541 (2017) 434–446.
782 https://doi.org/10.1016/j.memsci.2017.07.015.
783 [14] K.L. Tu, L.D. Nghiem, A.R. Chivas, Coupling effects of feed solution pH and ionic
784 strength on the rejection of boron by NF/RO membranes, Chem. Eng. J. 168 (2011) 700–
785 706. https://doi.org/10.1016/j.cej.2011.01.101.

[15] A. Gorenflo, M. Brusilovsky, M. Faigon, B. Liberman, High pH operation in seawater reverse osmosis permeate: First results from the world's largest SWRO plant in Ashkelon, Desalination. 203 (2007) 82–90. https://doi.org/10.1016/j.desal.2006.05.004.

[16] B. Sauvet-goichon, Ashkelon desalination plant — A successful challenge, Desalination. 203 (2007) 75–81. https://doi.org/10.1016/j.desal.2006.03.525.

[17] Z. Guan, J. Lv, P. Bai, X. Guo, Boron removal from aqueous solutions by adsorption — A review, Desalination. 383 (2016) 29–37. https://doi.org/10.1016/j.desal.2015.12.026.

[18] J. Lin, N.N.N. Mahasti, Y. Huang, Recent advances in adsorption and coagulation for boron removal from wastewater: A comprehensive review, J. Hazard. Mater. 407 (2021) 124401. https://doi.org/10.1016/j.jhazmat.2020.124401.

[19] Y.P. Tang, T.S. Chung, M. Weber, C. Maletzko, Development of novel diol-functionalized silica particles toward fast and efficient boron removal, Ind. Eng. Chem. Res. 56 (2017) 11618–11627. https://doi.org/10.1021/acs.iecr.7b03115.

[20] J. Meng, J. Cao, R. Xu, Z. Wang, R. Sun, Hyperbranched grafting enabling simultaneous enhancement of the boric acid uptake and the adsorption rate of a complexing membrane, J. Mater. Chem. A. 4 (2016) 11656–11665. https://doi.org/10.1039/c6ta02348g.

[21] J. Kamcev, M.K. Taylor, D.M. Shin, N.N. Jarenwattananon, K.A. Colwell, J.R. Long, Functionalized porous aromatic frameworks as high-performance adsorbents for the rapid removal of boric acid from water, Adv. Mater. (2019) 1808027. https://doi.org/10.1002/adma.201808027.

[22] S. Kürklü, S. Velio, M. Göktu, S.B. Tantekin-ersolmaz, W.B. Krantz, A novel energy-efficient concurrent desalination and boron removal (CDBR) process, 423 (2017) 79–94. https://doi.org/10.1016/j.desal.2017.09.005.

[23] M.R. Landsman, D.F. Lawler, L.E. Katz, Application of electrodialysis pretreatment to enhance boron removal and reduce fouling during desalination by nanofiltration/reverse osmosis, Desalination. 491 (2020) 114563. https://doi.org/10.1016/j.desal.2020.114563.

[24] Z. Ali, Y. Al Sunbul, F. Pacheco, W. Ogieglo, Y. Wang, G. Genduso, I. Pinnau, Defect-free highly selective polyamide thin-film composite membranes for desalination and boron removal, J. Memb. Sci. 578 (2019) 85–94. https://doi.org/10.1016/j.memsci.2019.02.032.

[25] Y. Li, S. Wang, X. Song, Y. Zhou, H. Shen, X. Cao, P. Zhang, C. Gao, High boron removal polyamide reverse osmosis membranes by swelling induced embedding of a sulfonyl molecular plug, J. Memb. Sci. 597 (2020) 117716. https://doi.org/10.1016/j.memsci.2019.117716.

[26] R. Bernstein, S. Belfer, V. Freger, Toward improved boron removal in RO by membrane modification: Feasibility and challenges, Environ. Sci. Technol. 45 (2011) 3613–3620. https://doi.org/10.1021/es103991u.

[27] S. Shultz, M. Bass, R. Semiat, V. Freger, Modification of polyamide membranes by hydrophobic molecular plugs for improved boron rejection, J. Memb. Sci. 546 (2018) 165–172. https://doi.org/10.1016/j.memsci.2017.10.003.

[28] S. Wang, Y. Zhou, C. Gao, Novel high boron removal polyamide reverse osmosis membranes, J. Memb. Sci. 554 (2018) 244–252. https://doi.org/10.1016/j.memsci.2018.03.014.

[29] B. Jung, C.Y. Kim, S. Jiao, U. Rao, A. V. Dudchenko, J. Tester, D. Jassby, Enhancing boron rejection on electrically conducting reverse osmosis membranes through local electrochemical pH modification, Desalination. 476 (2020) 114212.

https://doi.org/10.1016/j.desal.2019.114212.

[30] H. Yamagishi, K. Saito, S. Furusaki, T. Sugo, I. Ishigaki, Introduction of a high-density chelating group into a porous membrane without lowering the flux, Ind. Eng. Chem. Res. 30 (1991) 2234–2237. https://doi.org/10.1021/ie00057a028.

[31] Y. Zhang, J.R. Vallin, J.K. Sahoo, F. Gao, B.W. Boudouris, M.J. Webber, W.A. Phillip, High-affinity detection and capture of heavy metal contaminants using block polymer composite membranes, ACS Cent. Sci. 4 (2018) 1697–1707. https://doi.org/10.1021/acscentsci.8b00690 ACS.

[32] J.R. Hoffman, W.A. Phillip, 100th anniversary of macromolecular science viewpoint: Integrated membrane systems, ACS Macro Lett. 9 (2020) 1267–1279. https://doi.org/10.1021/acsmacrolett.0c00482.

[33] R. Sujanani, M.R. Landsman, S. Jiao, J.D. Moon, M.S. Shell, D.F. Lawler, L.E. Katz, B.D. Freeman, Designing solute-tailored selectivity in membranes: Perspectives for water reuse and resource recovery, ACS Macro Lett. 9 (2020) 1709–1717. https://doi.org/10.1021/acsmacrolett.0c00710.

[34] N. Bachelier, C. Chappey, D. Langevin, M. M, J. Verch, Facilitated transport of boric acid by 1,3-diols through supported liquid membranes, J. Memb. Sci. 119 (1996) 285–294.

[35] X. Du, J. Meng, R. Xu, Q. Shi, Y. Zhang, Polyol-grafted polysulfone membranes for boron removal: Effects of the ligand structure, J. Memb. Sci. 476 (2015) 205–215. https://doi.org/10.1016/j.memsci.2014.11.042.

[36] Z. Wang, Z. Wu, Y. Zhang, J. Meng, Hyperbranched-polyol-tethered poly (amic acid) electrospun nanofiber membrane with ultrahigh adsorption capacity for boron removal, Appl. Surf. Sci. 402 (2017) 21–30. https://doi.org/10.1016/j.apsusc.2017.01.070.

855 [37] F. Albertini, T. Ribeiro, S. Alves, C. Baleizão, J.P.S. Farinha, Boron-chelating membranes
856 based in hybrid mesoporous silica nanoparticles for water purification, Mater. Des. 141
857 (2018) 407–413. https://doi.org/10.1016/j.matdes.2018.01.001.
858 [38] M. Di Vincenzo, M. Barboiu, A. Tiraferri, Y.M. Legrand, Polyol-functionalized thin-film
859 composite membranes with improved transport properties and boron removal in reverse
860 osmosis, J. Memb. Sci. 540 (2017) 71–77. https://doi.org/10.1016/j.memsci.2017.06.034.
861 [39] A.A. Uliana, N.T. Bui, J. Kamcev, M.K. Taylor, J.J. Urban, J.R. Long, Ion-capture
862 electrodialysis using multifunctional adsorptive membranes, Science. 372 (2021) 296–
863 299. https://doi.org/10.1126/science.abf5991.
864 [40] J.G.G. Wijmans, R.W.W. Baker, The solution-diffusion model: A review, J. Memb. Sci.
865 107 (1995) 1–21. https://doi.org/10.1016/0376-7388(95)00102-I.
866 [41] B.F. Lee, M.J. Kade, J.A. Chute, N. Gupta, L.M. Campos, G.H. Fredrickson, E.J. Kramer,
867 N.A. Lynd, C.J. Hawker, Poly(allyl glycidyl ether)-A versatile and functional polyether
868 platform, J. Polym. Sci. Part A Polym. Chem. 49 (2011) 4498–4504.
869 https://doi.org/10.1002/pola.24891.
870 [42] N.E. Good, G.D. Winget, W. Winter, T.N. Connolly, S. Izawa, R.M. Singh, Hydrogen ion
871 buffers for biological research, Biochemistry. 5 (1966) 467–477.
872 https://doi.org/10.1021/bi00866a011.
873 [43] N. Bin Darwish, V. Kochkodan, N. Hilal, Boron removal from water with fractionized
874 Amberlite IRA743 resin, Desalination. 370 (2015) 1–6.
875 https://doi.org/10.1016/j.desal.2015.05.009.
876 [44] M. Simonnot, C. Castel, M. Nicolaiè, C. Rosin, M. Sardin, H. Jauffret, Boron removal
877 from drinking water with a boron selective resin: Is the treatment really selective?, Water

878 Res. 34 (2000) 109–116. https://doi.org/10.1016/S0043-1354(99)00130-X.
879 [45] DuPont, Product Data Sheet: AmberSep™ IRA743 Chelating Resin (Form No. 45-
880 D00805-en, Rev. 1), 2020.
881 [46] R.B. Baird, A.D. Eaton, E.W. Rice, Standard methods for the examination of water and
882 wastewater, 23rd Ed., American Public Health Association, Water Environment
883 Federation, and American Water Works Association, Washington, D.C., 2017.
884 [47] M. Galizia, F.M. Benedetti, D.R. Paul, B.D. Freeman, Monovalent and divalent ion
885 sorption in a cation exchange membrane based on cross-linked poly (p-styrene sulfonate-
886 co-divinylbenzene), J. Memb. Sci. 535 (2017) 132–142.
887 https://doi.org/10.1016/j.memsci.2017.04.007.
888 [48] H. Yasuda, C.E. Lamaze, L.D. Ikenberry, Permeability of solutes through hydrated
889 polymer membranes. Part I. Diffusion of sodium chloride, Die Makromol. Chemie. 118
890 (1968) 19–35. https://doi.org/10.1002/macp.1968.021180102.
891 [49] E.-S. Jang, J. Kamcev, K. Kobayashi, N. Yan, R. Sujanani, T.J. Dilenschneider, H. Bum,
892 D.R. Paul, B.D. Freeman, Influence of water content on alkali metal chloride transport in
893 cross-linked poly(ethylene glycol) diacrylate. 1. Ion sorption, Polymer. 178 (2019)
894 121554. https://doi.org/10.1016/j.polymer.2019.121554.
895 [50] R.M. Barrer, J.A. Barrie, J. Slater, Sorption and diffusion in ethyl cellulose. Part III.
896 Comparison between ethyl cellulose and rubber, J. Polym. Sci. 27 (1958) 177–197.
897 https://doi.org/10.1002/pol.1958.1202711515.
898 [51] D.R. Paul, Gas sorption and transport in glassy polymers, Berichte Der
899 Bunsengesellschaft Für Phys. Chemie. 83 (1979) 294–302.
900 https://doi.org/10.1002/bbpc.19790830403.

[52] J. Crank, The Mathematics of Diffusion, Oxford University Press, 1979.

[53] C.G. Rodriguez, M. Chwatko, J. Park, C.L. Bentley, B.D. Freeman, N.A. Lynd, Compositionally controlled polyether membranes via mono(μ-alkoxo)bis(alkylaluminum)-initiated chain-growth network epoxide polymerization: Synthesis and transport properties, Macromolecules. 53 (2020) 1191–1198. https://doi.org/10.1021/acs.macromol.9b02318.

[54] H. Lin, B.D. Freeman, Materials selection guidelines for membranes that remove CO_2 from gas mixtures, J. Mol. Struct. 739 (2005) 57–74. https://doi.org/10.1016/j.molstruc.2004.07.045.

[55] T. Brinkmann, J. Lillepärg, H. Notzke, J. Pohlmann, S. Shishatskiy, J. Wind, T. Wolff, Development of CO_2 selective poly(ethylene oxide)-based membranes: From laboratory to pilot plant scale, Engineering. 3 (2017) 485–493. https://doi.org/10.1016/J.ENG.2017.04.004.

[56] S. Bandehali, A. Moghadassi, F. Parvizian, Advances in high carbon dioxide separation performance of poly(ethylene oxide)-based membranes, J. Energy Chem. 46 (2020) 30–52. https://doi.org/10.1016/j.jechem.2019.10.019.

[57] K. Knop, R. Hoogenboom, D. Fischer, U.S. Schubert, Poly(ethylene glycol) in drug delivery: Pros and cons as well as potential alternatives, Angew. Chemie - Int. Ed. 49 (2010) 6288–6308. https://doi.org/10.1002/anie.200902672.

[58] Z. Xue, D. He, X. Xie, Poly(ethylene oxide)-based electrolytes for lithium-ion batteries, J. Mater. Chem. A. 3 (2015) 19218–19253. https://doi.org/10.1039/c5ta03471j.

[59] J. McMurry, Amines and heterocycles: Spectroscopy of amines, in: Org. Chem., 9th Ed., Cengage Learning, Boston, MA, 2015.

924 [60] G.M. Geise, D.R. Paul, B.D. Freeman, Fundamental water and salt transport properties of
925 polymeric materials, Prog. Polym. Sci. 39 (2014) 1–42.
926 https://doi.org/10.1016/j.progpolymsci.2013.07.001.
927 [61] H. Ju, A.C. Sagle, B.D. Freeman, J.I. Mardel, A.J. Hill, Characterization of sodium
928 chloride and water transport in crosslinked poly (ethylene oxide) hydrogels, J. Memb.
929 Sci. 358 (2010) 131–141. https://doi.org/10.1016/j.memsci.2010.04.035.
930 [62] X. Zhang, J. Wang, S. Chen, Z. Bao, H. Xing, Z. Zhang, B. Su, Q. Yang, Y. Yang, Q.
931 Ren, A spherical N-methyl-D-glucamine-based hybrid adsorbent for highly efficient
932 adsorption of boric acid from water, Sep. Purif. Technol. 172 (2017) 43–50.
933 https://doi.org/10.1016/j.seppur.2016.08.002.
934 [63] G.N. Manjunatha Reddy, J.A. Gerbec, F. Shimizu, B.F. Chmelka, Nanoscale surface
935 compositions and structures influence boron adsorption properties of anion exchange
936 resins, Langmuir. 35 (2019) 15661–15673. https://doi.org/10.1021/acs.langmuir.9b02042.
937 [64] J. Wang, Y. Zhang, Boronic acids as hydrogen bond donor catalysts for efficient
938 conversion of CO_2 into organic carbonate in water, ACS Catal. 6 (2016) 4871–4876.
939 https://doi.org/10.1021/acscatal.6b01422.
940 [65] Y. Ye, D. Li, P. Xu, J. Sun, B-doped and NH_2-functionalized SBA-15 with hydrogen bond
941 donor groups for effective catalysis of CO_2 cycloaddition to epoxides, Inorg. Chem. Front.
942 7 (2020) 3636–3645. https://doi.org/10.1039/d0qi00703j.
943 [66] L. Zhao, J. Chen, W. Li, A. Lu, B_2O_3: A heterogeneous metal-free Lewis acid catalyst for
944 carbon dioxide fixation into cyclic carbonates, J. CO_2 Util. 29 (2019) 172–178.
945 https://doi.org/10.1016/j.jcou.2018.12.006.
946 [67] A.Z. Halimehjani, H. Gholami, M.R. Saidi, Boric acid/glycerol as an efficient catalyst for

regioselective epoxide ring opening by aromatic amines in water, Green Chem. Lett. Rev. 5 (2012) 1–5. https://doi.org/10.1080/17518253.2011.572297.

[68] M. Pineschi, Boron reagents and catalysts for the functionalization of strained heterocycles, Adv. Synth. Catal. 363 (2021) 2325–2339. https://doi.org/10.1002/adsc.202001493.

[69] Y.J. Kim, S.H. Choi, S.J. Lee, K. Jang, Latent curing, chemorheological, kinetic, and thermal behaviors of epoxy resin matrix for prepregs, Ind. Eng. Chem. Res. (2021). https://doi.org/10.1021/acs.iecr.1c00576.

[70] F. Risplendi, F. Ra, L. Lin, C. Grossman, Fundamental insights on hydration environment of boric acid and its role in separation from saline water, J. Phys. Chem. C. 124 (2020) 1438–1445. https://doi.org/10.1021/acs.jpcc.9b10065.

[71] N. Ingri, G. Lagerström, M. Frydman, L.G. Sillén, Equilibrium studies of polyanions. II. Polyborates in $NaClO_4$ medium, Acta Chem. Scand. 11 (1957) 1034–1058. https://doi.org/10.3891/acta.chem.scand.11-1034.

[72] J. Wang, R.S. Kingsbury, L.A. Perry, O. Coronell, Partitioning of alkali metal salts and boric acid from aqueous phase into the polyamide active layers of reverse osmosis membranes, Environ. Sci. Technol. 51 (2017) 2295–2303. https://doi.org/10.1021/acs.est.6b04323.

[73] T. Itou, H. Kitai, A. Shimazu, T. Miyazaki, K. Tashiro, Clarification of cross-linkage structure in boric acid doped poly(vinyl alcohol) and its model compound as studied by an organized combination of X-ray single-crystal structure analysis, Raman spectroscopy, and density functional theoretical calculation, J. Phys. Chem. B. 118 (2014) 6032–6037. https://doi.org/10.1021/jp5026569.

970 [74] A. Roy, A. Choudhury, C.N.R. Rao, Supramolecular hydrogen-bonded structure of a 1:2
971 adduct of melamine with boric acid, J. Mol. Struct. 613 (2002) 61–66.
972 https://doi.org/10.1016/S0022-2860(02)00128-X.
973 [75] B. Mi, B.J. Marin, D.G. Cahill, RBS characterization of arsenic(III) partitioning from
974 aqueous phase into the active layers of thin-film composite NF/RO membranes, Env. Sci
975 Technol. 41 (2007) 3290–3295. https://doi.org/10.1021/es062292v.
976 [76] D. Peak, G.W.G.W.I. Luther, D.L.D.L. Sparks, ATR-FTIR spectroscopic studies of boric
977 acid adsorption on hydrous ferric oxide, Geochim. Cosmochim. Acta. 67 (2003) 2551–
978 2560. https://doi.org/10.1016/S0016-7037(03)00096-6.
979 [77] K. Yoshimura, Y. Miyazaki, F. Ota, S. Matsuoka, H. Sakashita, Complexation of boric
980 acid with the N-methyl-D-glucamine group in solution and in crosslinked polymer, J.
981 Chem. Soc. - Faraday Trans. 94 (1998) 683–689. https://doi.org/10.1039/a707790d.
982 [78] M.P. Schmidt, S.D. Siciliano, D. Peak, The role of monodentate tetrahedral borate
983 complexes in boric acid binding to a soil organic matter analogue, Chemosphere. 276
984 (2021) 130150. https://doi.org/10.1016/j.chemosphere.2021.130150.
985 [79] T. Ide, Y. Hirayama, How boron is adsorbed by D-glucamine: A density functional theory
986 study, Comput. Theor. Chem. 1150 (2019) 85–90.
987 https://doi.org/10.1016/j.comptc.2019.01.007.
988 [80] C. Sanfeliu, R. Martínez-Máñez, F. Sancenón, J. Soto, P. Amorós, T. Azaïs, M.D. Marcos,
989 11B-MAS NMR approach to the boron adsorption mechanism on a glucose-functionalised
990 mesoporous silica matrix, Microporous Mesoporous Mater. 266 (2018) 232–241.
991 https://doi.org/10.1016/j.micromeso.2018.02.016.
992 [81] E. Ruckenstein, A.S. Vaidyanathan, G.R. Youngquist, Sorption by solids with bidisperse

pore structures, Chem. Eng. Sci. 26 (1971) 1305–1318. https://doi.org/10.1016/0009-2509(71)80051-9.

[82] M. Laatikainen, M. Lindstrcm, Measurement of sorption in polymer membranes with a quartz crystal microbalance, J. Memb. Sci. 29 (1986) 127–141. https://doi.org/10.1016/S0376-7388(00)82464-3.

[83] M.D. Placette, X. Fan, J.-H. Zhao, D. Edwards, A dual stage model of anomalous moisture diffusion and desorption in epoxy mold compounds, 2011 12th Intl. Conf. Therm. Mech. Multi-Physics Simul. Exp. Microelectron. Microsystems. (2011) 1–8. https://doi.org/10.1109/ESIME.2011.5765824.

[84] C.C. McDowell, B.D. Freeman, G.W. McNeely, Acetone sorption and uptake kinetic in poly(ethylene terephthalate), Polymer. 40 (1999) 3487–3499.

[85] E. Jang, J. Kamcev, K. Kobayashi, N. Yan, R. Sujanani, T.J. Dilenschneider, H. Bum, D.R. Paul, B.D. Freeman, Influence of water content on alkali metal chloride transport in cross-linked Poly(ethylene glycol) diacrylate. 2. Ion diffusion, Polymer. 192 (2020) 122316. https://doi.org/10.1016/j.polymer.2020.122316.

[86] M. Galizia, D.R. Paul, B.D. Freeman, Liquid methanol sorption, diffusion and permeation in charged and uncharged polymers, Polymer. 102 (2016) 281–291. https://doi.org/10.1016/j.polymer.2016.09.010.

[87] J.S. Mackie, P. Meares, The diffusion of electrolytes in a cation-exchange resin membrane. I. Theoretical, Proc. R. Soc. London, Ser. A. 232 (1955) 498–509. https://doi.org/10.1098/rspa.1955.0234.

[88] W. Huang, W.J. Weber, A Distributed reactivity model for sorption by soils and sediments. 10. Relationships between desorption, hysteresis, and the chemical

characteristics of organic domains, Env. Sci Technol. 31 (1997) 2562–2569. https://doi.org/10.1021/es960995e.

[89] A.T. Kan, G. Fu, M.B. Tomson, Adsorption/desorption hysteresis in organic pollutant and soil/sediment interaction, Env. Sci Technol. 28 (1994) 859–867. https://doi.org/10.1021/es00054a017.

[90] X. Cheng, A.T. Kan, M.B. Tomson, Naphthalene adsorption and desorption from aqueous C-60 fullerene, J. Chem. Eng. Data. 49 (2004) 675–683. https://doi.org/10.1021/je030247m.

[91] D.E. Liu, T.J. Dursch, N.O. Taylor, S.Y. Chan, D.T. Bregante, C.J. Radke, Diffusion of water-soluble sorptive drugs in HEMA/MAA hydrogels, J. Control. Release. 239 (2016) 242–248. https://doi.org/10.1016/j.jconrel.2016.08.025.

[92] J.A. Tshudy, C. von Frankenberg, A model incorporating reversible immobilization for sorption and diffusion in glassy polymers, J. Polym. Sci. 11 (1973) 2027–2037. https://doi.org/10.1002/pol.1973.180111012.

[93] A. Gennari, C. Gujral, E. Hohn, E. Lallana, F. Cellesi, N. Tirelli, Revisiting Boronate/Diol Complexation as a Double Stimulus- Responsive Bioconjugation, Bioconjug. Chem. 28 (2017) 1391–1402. https://doi.org/10.1021/acs.bioconjchem.7b00080.

[94] R. Barati, J.T. Liang, A review of fracturing fluid systems used for hydraulic fracturing of oil and gas wells, J. Appl. Polym. Sci. 131 (2014) 1–11. https://doi.org/10.1002/app.40735.

[95] T. Bu, F. Chen, X. He, Y. Yang, W. Wang, Researching the complexing conditions of residual boron in produced water from oil & gas fields, Process Saf. Environ. Prot. 116 (2018) 254–261. https://doi.org/10.1016/j.psep.2018.02.013.

[96] S.D. Bull, M.G. Davidson, J.M.H. van den Elsen, J.S. Fossey, A.T.A. Jenkins, Y. Jiang, Y. Kubo, F. Marken, K. Sakurai, J. Zhao, T.D. James, Exploiting the reversible covalent bonding of boronic acids: Recognition, sensing, and assembly, Acc. Chem. Res. 46 (2013) 312–326. https://doi.org/10.1021/ar300130w.

[97] B. Marco-Dufort, M.W. Tibbitt, Design of moldable hydrogels for biomedical applications using dynamic covalent boronic esters, Mater. Today Chem. 12 (2019) 16–33. https://doi.org/10.1016/j.mtchem.2018.12.001.

[98] S.Y. Lee, M. Yang, J. Seo, D.I. Jeong, C. Hwang, H. Kim, J. Lee, K. Lee, J. Park, H. Cho, Serially pH-modulated hydrogels based on boronate ester and polydopamine linkages for local cancer therapy, ACS Appl. Mater. Interfaces. 13 (2021) 2189–2203. https://doi.org/10.1021/acsami.0c16199.

[99] P. Millner, High Resolution Chromatography: A Practical Approach, Oxford University Press, 1999.

[100] Dionex, Product Manual: IonPac TBC-1 Trace Borate Concentrator Column and IonPac ICE-Borate IC Column, Sunnyvale, CA, 2004.

[101] S. Bonollo, D. Lanari, L. Vaccaro, Ring-opening of epoxides in water, European J. Org. Chem. (2011) 2587–2598. https://doi.org/10.1002/ejoc.201001693.